Control of bone resorption in mice by Schnurri-3

Marc N. Wein[a,b], Dallas C. Jones[a], Jae-Hyuck Shim[a], Antonios O. Aliprantis[a,c], Rosalyn Sulyanto[a], Vanja Lazarevic[a], Sandra L. Poliachik[d], Ted S. Gross[d], and Laurie H. Glimcher[a,c,e,f,1,2]

[a]Department of Immunology and Infectious Disease, Harvard School of Public Health, Boston, MA 02115; [d]Department of Orthopedics and Sports Medicine, University of Washington, Seattle, WA 98104; [b]Endocrine Unit, Massachusetts General Hospital, Boston, MA 02114; [c]Division of Rheumatology, Allergy, and Immunology, Department of Medicine, Brigham and Women's Hospital, Harvard Medical School, Boston, MA 02115; [e]Department of Medicine, Harvard Medical School, Boston, MA 02115; and [f]Ragon Institute of Massachusetts Institute of Technology, Massachusetts General Hospital and Harvard University, Charlestown, MA 02129

Contributed by Laurie H. Glimcher, April 9, 2012 (sent for review March 5, 2012)

Mice lacking the large zinc finger protein Schnurri-3 (Shn3) display increased bone mass, in part, attributable to augmented osteoblastic bone formation. Here, we show that in addition to regulating bone formation, Shn3 indirectly controls bone resorption by osteoclasts in vivo. Although Shn3 plays no cell-intrinsic role in osteoclasts, Shn3-deficient animals show decreased serum markers of bone turnover. Mesenchymal cells lacking Shn3 are defective in promoting osteoclastogenesis in response to selective stimuli, likely attributable to reduced expression of the key osteoclastogenic factor receptor activator of nuclear factor-κB ligand. The bone phenotype of Shn3-deficient mice becomes more pronounced with age, and mice lacking Shn3 are completely resistant to disuse osteopenia, a process that requires functional osteoclasts. Finally, selective deletion of Shn3 in the mesenchymal lineage recapitulates the high bone mass phenotype of global Shn3 KO mice, including reduced osteoclastic bone catabolism in vivo, indicating that Shn3 expression in mesenchymal cells directly controls osteoblastic bone formation and indirectly regulates osteoclastic bone resorption.

cAMP response element binding protein | receptor activator of nuclear factor-κB ligand | secondary hyperparathyroidism

Schnurri-3 (Shn3) is a large zinc finger protein belonging to the small group of zinc finger, acid-rich, and serine-threonine rich (ZAS) family proteins (1). Previous in vitro studies have implicated a role for Shn3 in diverse processes, such as Ig gene rearrangement, cell survival, TNF signaling in macrophages, and IL-2 gene expression in helper T lymphocytes (2–6). We recently discovered that mice with germline deletion of Shn3 displayed a massive increase in bone mass, revealing an unexpected role for this protein in the skeletal system (5). Shn3-deficient animals showed markedly augmented osteoblastic bone formation in vivo. Consistently, cultured primary osteoblasts lacking Shn3 express increased levels of classic osteoanabolic genes and produce increased amounts of mineralized ECM. In osteoblasts, Shn3 functions, at least in part, by regulating Runx2 protein levels via its ubiquitination.

A central dogma in skeletal biology is that bone formation and resorption are coupled, such that manipulations that increase bone production by osteoblasts typically increase bone catabolism by osteoclasts (7–9). Pharmacological augmentation of bone production in humans with recombinant parathyroid hormone (PTH) leads to a compensatory increase in serum markers of bone turnover. Likewise, inhibition of bone resorption following bisphosphonate or denosumab treatment leads to decreased bone production (10, 11). In most murine models of increased bone production attributable to osteoblast-intrinsic manipulations, a compensatory increase in osteoclastic activity is typically seen (12, 13). However, this is not always the case (14–16). Although the mechanisms controlling mesenchymal/osteoclast cross-talk are incompletely understood, expression of the crucial osteoclastogenic factors *TNFSF11* [receptor activator of nuclear factor-κB ligand (RANKL)] and *TNFRSF11B* [osteoprotegerin (OPG)] by chondrocytes, osteoblasts, stromal cells, and osteocytes plays a dominant role (17–19).

Here, we show that in addition to increased bone formation, Shn3-deficient mice display a paradoxical reduction in osteoclastic bone resorption attributable to an osteoclast-extrinsic mechanism. In addition to producing increased amounts of mineralized ECM, Shn3-deficient stromal/osteoblastic cells are defective in driving osteoclastogenesis in vitro. We show that Shn3 controls expression of RANKL in mesenchymal cells.

Shn3-deficient mice continue to accrue bone with aging even when bone formation rates are no longer elevated. Shn3-deficient mice fail to lose bone in a disuse model of osteolysis. In addition, although deletion of the master regulator of osteoclastogenesis, NFATc1, increases cortical bone mass in WT mice, it has no effect in the presence of Shn3 deficiency, supporting the contention that Shn3-deficient mice have a marked basal reduction in osteoclastogenesis. Finally, selective mesenchymal deletion of Shn3 with Prx1-Cre recapitulates the observed skeletal phenotype of global Shn3 deletion, including reduced osteoclast numbers and reduced bone catabolism in vivo.

Results

We previously demonstrated that the adult-onset high bone mass phenotype of mice lacking Shn3 persists following WT bone marrow (BM) transplantation, and that Shn3-deficient BM cells display normal osteoclast differentiation and resorptive function in vitro (5). To rule out a role for Shn3 in regulating bone resorption in an osteoclast-intrinsic manner further, we performed reciprocal BM transplantation experiments. Good hematopoietic chimerism was achieved (Fig. S1*A*), and, as expected, the Shn3-deficient high bone mass phenotype mapped to the genotype of the host animal (Fig. S1*B*). We conclude that Shn3 deficiency exerts its effect on bone mass through its expression in a radioresistant (i.e., nonosteoclast) cell type in vivo.

Reduced Osteoclast Activity in Shn3-Deficient Mice in Vivo. We sought to characterize osteoclast activity in Shn3$^{-/-}$ mice further in vivo. Because these animals show dramatic elevations in osteoblast behavior as assayed by dynamic histomorphometry (5), we predicted that these mice might show a compensatory increase in serum markers of bone resorption. This was not the case. As shown in Fig. 1 *A* and *B*, serum markers of collagen type 1 cross-linked C-telopeptide (CTX) and Pyd were significantly reduced in young (6-wk-old) Shn3$^{-/-}$ animals compared with WT littermates.

Previously, we reported comparable numbers of osteoclasts in WT and Shn3$^{-/-}$ skeletal tissue as assessed by histomorphometry just below the growth plate in the proximal tibia (5). Given the unexpected decrease in markers of bone resorption, we performed a more extensive histochemical investigation and observed qualitative reductions in osteoclast numbers in whole-mount skull preparations (Fig. 1*C*) and along the surfaces of increased diaphyseal trabecular bone (Fig. 1*D*) in Shn3$^{-/-}$ animals.

Author contributions: M.N.W., D.C.J., J.-H.S., A.O.A., R.S., V.L., S.L.P., T.S.G., and L.H.G. designed research; M.N.W., D.C.J., J.-H.S., A.O.A., R.S., V.L., S.L.P., and T.S.G. performed research; M.N.W., D.C.J., J.-H.S., A.O.A., R.S., V.L., S.L.P., T.S.G., and L.H.G. analyzed data; and M.N.W., D.C.J., and L.H.G. wrote the paper.

The authors declare no conflict of interest.

[1]Present address: Dean's Office, Weill Cornell Medical College, New York, NY 10021.

[2]To whom correspondence should be addressed. E-mail: lglimche@med.cornell.edu.

This article contains supporting information online at www.pnas.org/lookup/suppl/doi:10.1073/pnas.1205848109/-/DCSupplemental.

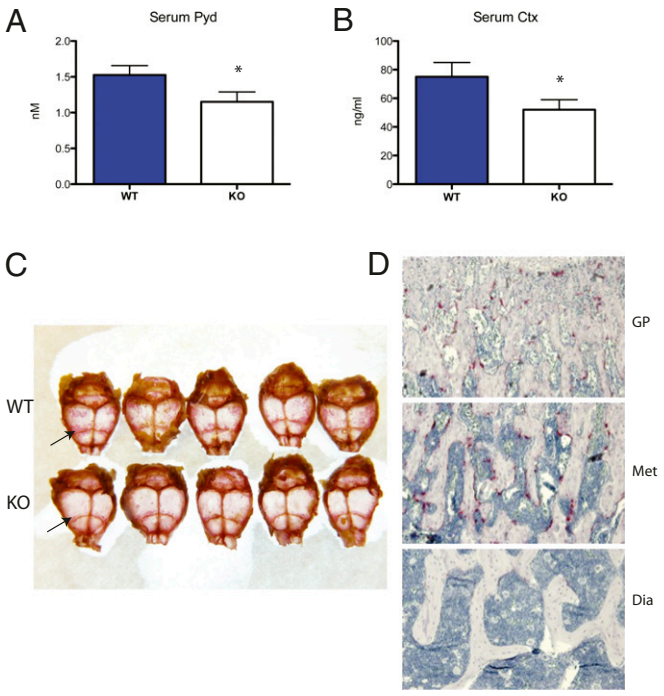

Fig. 1. Decreased bone resorption in Shn3-deficient mice. (*A*) Serum Pyd levels in 6-wk-old WT and Shn3$^{-/-}$ (KO) animals (n = 6 per group). *$P < 0.05$ comparing WT with KO animals. (*B*) Serum CTX levels levels in 6-wk-old WT and KO animals (n = 10 per group). (*C*) Representative photograph of whole-mount TRAP stain (pink, arrows highlight prominent staining near sutures) of WT and KO 8-wk-old skull preparations. (*D*) Representative photomicrographs of an 8-wk-old Shn3$^{-/-}$ femur section stained for TRAP (pink) at the growth plate (GP; *Top*), distal metaphyseal (Met; *Middle*), and diaphyseal (Dia; *Bottom*) section levels. (Magnification: 10×.)

Interestingly, this analysis confirmed normal numbers of osteoclasts just below the growth plate in the tibiae and femurs of Shn3$^{-/-}$ animals, suggesting that Shn3 may control osteoclast numbers and/or activity in a skeletal region-selective manner. In Fig. 1*D*, WT control sections were not analyzed because of the drastically different qualitative nature of bone mass and quality at the diaphyseal level. Taken together, these data suggest that Shn3 expression in nonosteoclastic cells may regulate osteoclast development and/or activity.

Mesenchymal Cells Lacking Shn3 Are Defective in Driving Osteoclastogenesis. Radioresistant cells of stromal/osteoblastic lineage are known to support osteoclast development in vitro in response to calciotropic stimuli by expression of RANKL (18–21). To interrogate the ability of Shn3-deficient cells to support osteoclastogenesis, we performed coculture experiments. In these assays, we observed that osteoblastic/stromal cells lacking Shn3 were defective in driving osteoclastogenesis in response to prostaglandin E2 (PGE2) and the β2-adrenergic receptor agonist isoproterenol but not PTH (Fig. 2*A*). We did not specifically address the resorptive capacity of the osteoclasts generated during these in vitro coculture assays. However, we do note that mice lacking Shn3 (Fig. 1 *A* and *B*; see Fig. 5*J*) display reduced serum markers of bone turnover, indicating reduced osteoclast activity in vivo.

Morphological analysis of osteoclasts from these coculture assays revealed a consistent lack of giant multinucleated cells in the presence of Shn3$^{-/-}$ stromal cells (Fig. 2*B*). Consistent with this, RNA obtained from these cocultures showed reduced expression of terminal markers of osteoclast differentiation (cathepsin K and calcitonin receptor) comparing WT with Shn3$^{-/-}$ stromal cells/osteoblasts (Fig. 2*C*).

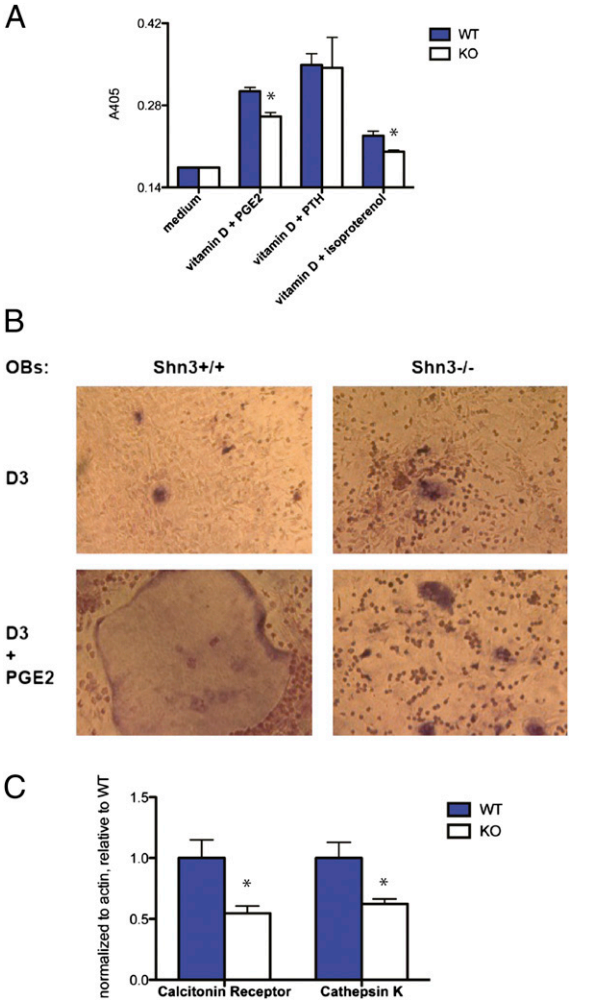

Fig. 2. Shn3-deficient osteoblastic/mesenchymal cells are defective in driving osteoclastogenesis. (*A*) WT or Shn3$^{-/-}$ cells were cocultured with WT BM osteoclast precursors in the presence of the indicated calciotropic agents. After 5 d, tissue culture supernatants were assayed for TRAP activity via colorimetric readout (A405). Error bars represent SD of absorbance from three independent wells. *$P < 0.05$. This experiment was repeated four independent times with similar results. (*B*) Representative photomicrographs of cocultures. (Magnification: 40×.) (*C*) RNA was harvested from cocultures, and expression of calcitonin receptor and cathepsin K was determined by quantitative real-time PCR assay. Levels of the indicated genes were normalized to actin and expressed relative to levels obtained with WT osteoblastic cells. Error bars represent SD of values obtained from PCR triplicate assays. This experiment was repeated three independent times with similar results.

Reduced Levels of RANKL in the Absence of Shn3 in Vivo. We next turned our attention to understanding the mechanism(s) whereby Shn3 expression in osteoblastic/stromal cells might control osteoclast differentiation. To this end, we performed RNA profiling to determine genes controlled by Shn3. In doing so, we found that the critical osteoclastogenic cytokine *TNFSF11* (RANKL) is one such gene whose levels are significantly decreased in Shn3$^{-/-}$ bone tissue (Fig. 3*A*). Serum analysis showed reduced circulating levels of RANKL in Shn3-deficient animals (Fig. 3*B*).

To explore the expression pattern of RANKL in bone tissue lacking Shn3 further, we performed immunohistochemistry for RANKL and histochemical labeling for the osteoclast marker tartrate resistant acid phosphatase (TRAP). These studies demonstrated comparable levels of RANKL in growth plate hypertrophic chondrocytes (Fig. S2*A*) and p10 proximal metaphyseal bone lining cells (Fig. S2*B*) but qualitatively reduced levels of RANKL and TRAP in bone lining cells more distant from the

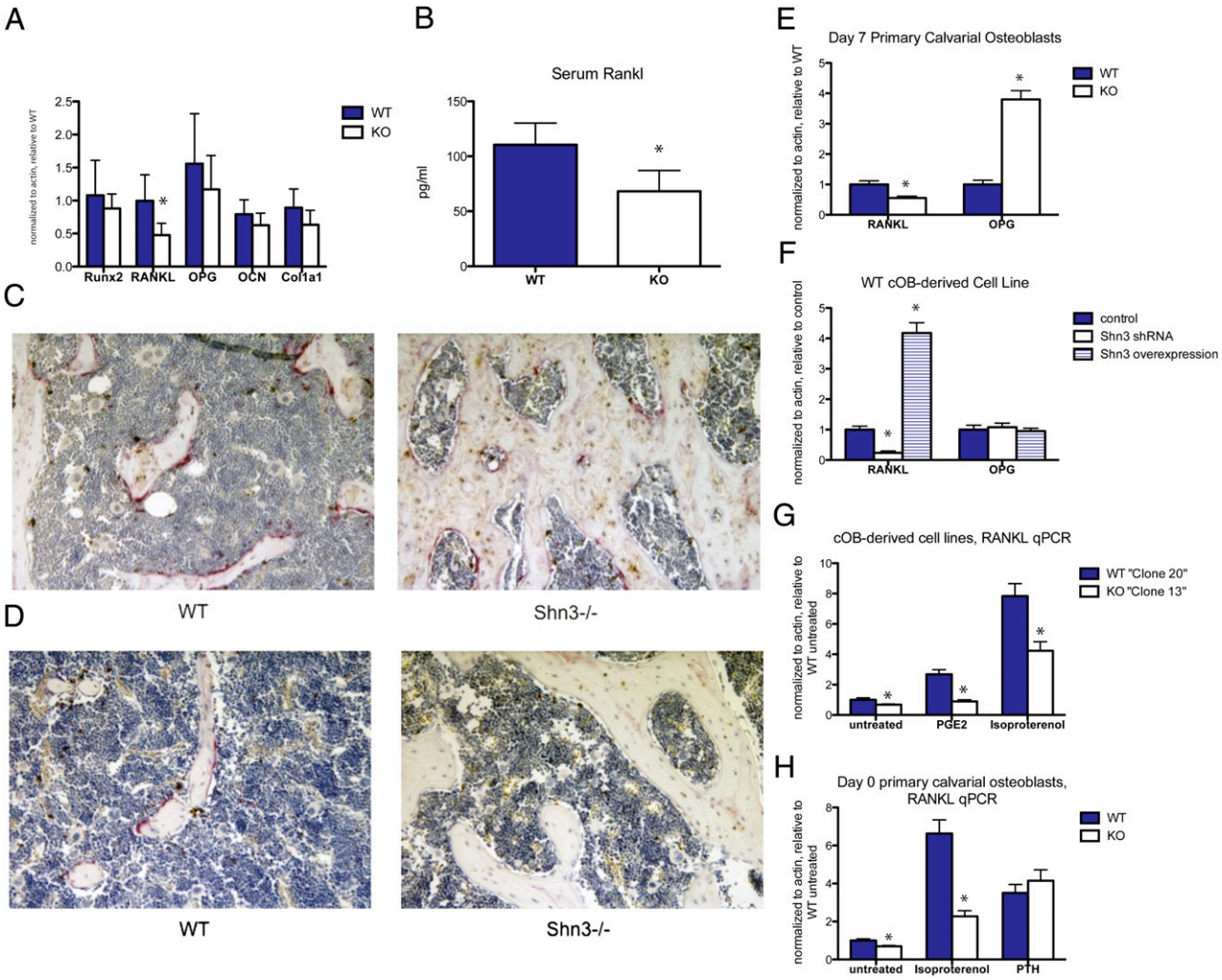

Fig. 3. Decreased RANKL in Shn3-deficient mice and cells. (*A*) RNA was isolated from calvariae of WT and Shn3$^{-/-}$ (KO) 8-wk-old mice (n = 5 mice per genotype). Transcript levels of the indicated genes were determined relative to actin by quantitative PCR assay and expressed as normalized to WT. Error bars represent SD values. *$P < 0.05$. The only gene showing significant change between WT and KO was RANKL. OCN, osteocalcin. (*B*) Serum RANKL was determined from 8-wk-old WT and KO mice (n = 10 mice per genotype). *$P < 0.01$. (*C*) Representative photomicrographs from femurs from 8-wk-old WT and Shn3$^{-/-}$ mice were costained for RANKL immunohistochemistry (IHC) (brown) and TRAP (pink) at the distal metaphysis. (*D*) Representative diaphyseal sections. Note the paucity of TRAP reactivity and RANKL-immunoreactive cells at this level. (*E*) Primary calvarial-derived osteoblasts from WT and KO mice were grown in culture for 7 d. RNA was isolated, and transcript levels of RANKL and OPG were determined relative to actin. *$P < 0.05$. (*F*) SV40-transformed WT calvarial osteoblast cell line was infected with either control lentivirus, Shn3 shRNA lentivirus, or Shn3 overexpression (N3557) lentivirus. RNA was isolated, and RANKL/OPG levels were determined relative to actin. (*G*) SV40-transformed WT (clone 20) and Shn3$^{-/-}$ (clone 13) cells were treated with the indicated agent for 90 min, and RANKL RNA levels were determined. (*H*) Day 0 primary calvarial osteoblasts were treated with the indicated agents for 3 h, and RANKL levels were determined. (Magnification: 10× in *C* and *D*.)

growth plate [Fig. 3 *C* (metaphyseal region) and *D* (diaphyseal region)]. Another cell type known to express RANKL is the CD4$^+$ T helper 17 (Th17) cell (22). Shn3 is dispensable for Th17 cell differentiation and RANKL expression (Fig. S2*C*). Taken together, these data indicate that Shn3 controls RANKL expression by osteoblastic/stromal cells in vivo but not in hypertrophic chondrocytes and Th17 cells.

Reduced Expression of RANKL by Osteoblastic/Stromal Cells Lacking Shn3. Primary calvarial osteoblasts lacking Shn3 show reduced levels of RANKL mRNA after a 7-d in vitro culture period. These cells also display increased levels of the antiosteoclastogenic factor OPG compared with WT cells (Fig. 3*E*). However, RANKL levels are known to decrease, and OPG levels to increase, during the course of osteoblast differentiation using this in vitro system (23). To circumvent the possibility that the differences observed reflect disparate differentiation states, we acutely altered Shn3 levels in transformed osteoblast cell lines using lentivirus-based shRNA-mediated gene silencing and overexpression. As shown in Fig. 3*F*, these manipulations led to the previously observed alterations in RANKL levels but not in OPG levels.

As shown in Fig. 2*A*, Shn3-deficient osteoblastic cells fully support osteoclastogenesis in response to PTH but not in response to isoproterenol and PGE2. Accordingly, Shn3$^{-/-}$ osteoblastic cells are defective in up-regulating RANKL in response to isoproterenol and PGE2 but not in response to PTH (Fig. 3 *G* and *H*). Acute reductions in Shn3 levels by shRNA-mediated gene silencing reduced responsiveness to PGE2 as expected (Fig. S3*A*). When coculture experiments were performed in the presence of a neutralizing anti-OPG antibody, the defect in the ability of Shn3$^{-/-}$ osteoblasts to drive osteoclastogenesis was reversed (Fig. S3*B*), suggesting that reduced RANKL expression by these cells contributes to their inability to support osteoclast differentiation.

Shn3 Controls Expression of RANKL Through cAMP Response Element Binding Protein and an Upstream Regulatory Element. We next sought to determine the mechanism whereby Shn3 controls RANKL expression. *TNFSF11* gene expression is controlled by a variety of distal and proximal regulatory regions (21, 24, 25). We focused on a conserved regulatory region located 76 kb upstream of the transcriptional start site that had been described by two independent groups as important for calciotropic agent responsiveness in vitro and in vivo (26). Shn3 overexpression can enhance activity of this upstream promoter element but not that of the proximal RANKL and OPG gene regulatory regions (Fig. S4*A*).

Transcription factors, such as vitamin D receptor (VDR), Runx2, cAMP response element binding protein (CREB), and STAT3, are known to associate with this RANKL gene regulatory region (24, 27). We found that Shn3 does not activate transcription from this reporter when the CREB binding sites are deleted (Fig. S4*B*). In overexpression studies, Shn3 can bind CREB (Fig. S4*C*) and regulates its transcriptional activity (Fig. S4 *D* and *E*). Taken together, these data suggest that Shn3 controls RANKL expression in osteoblastic cells in vivo and in vitro, at least in part, through a mechanism that involves binding to CREB in the context of a conserved upstream regulatory region.

Shn3-Deficient Animals Are Protected from Bone Loss Attributable to Aging and Disuse but Not Secondary Hyperparathyroidism. To explore the functional impact of RANKL regulation by Shn3 further, three models of stimulated bone resorption were used: aging, dietary-induced hypocalcemia, and disuse osteopenia. Young (8-wk-old) Shn3$^{-/-}$ mice show high bone mass associated with an increased rate of bone formation and decreased resorptive markers (5) (Fig. 1 *B* and *C*). Interestingly, aged (>3-mo-old) Shn3$^{-/-}$ animals continue to accrue bone, ultimately leading to obliteration of the marrow cavity and extramedullary hematopoiesis (not shown) but display reduced histomorphometric indices of bone formation (Fig. 4*A*). This phenotype of increasing bone mass with reduced bone formation rates in aged Shn3$^{-/-}$ mice is associated with reduced serum levels of the resorptive markers Pyd and CTX and RANKL (Fig. S5*A*). These findings suggest that the continued accrual of bone mass in aged Shn3$^{-/-}$ mice is driven by reduced bone resorption. Therefore, it appears that the cause of the high bone mass phenotype in Shn3-deficient mice varies with age. Young mice lacking Shn3 predominantly display an osteoanabolic phenotype, although as the mice age, bone formation slows down and the major phenotype is that of reduced bone resorption. Further studies are required to identify and dissect the age-related switch whereby this transition occurs.

Because PTH was able to increase RANKL expression normally in Shn3-deficient osteoblastic/mesenchymal cells, we wondered whether secondary hyperparathyroidism in vivo would lead to bone loss in Shn3-deficient mice. To test this notion, we placed 11-wk-old WT and Shn3$^{-/-}$ animals on a control diet or a low-calcium diet for 2 wk (28). Shn3$^{-/-}$ mice showed reductions in trabecular bone volume/total volume (BV/TV) (Fig. 4*B*) and increases in serum markers of bone resorption (Fig. S5*B*), and were able to maintain normocalcemia (Fig. S5*C*) in this model. Percent reductions in bone loss comparing WT with Shn3$^{-/-}$ mice were comparable. These data are consistent with our observations that Shn3 is dispensable for PTH-mediated induction of osteoclastogenesis in coculture models (Fig. 2*A*) and RANKL up-regulation in osteoblastic cells (Fig. 3*H*). Moreover, these data suggest that the Shn3$^{-/-}$ bone matrix is not "unresorbable," thereby discounting the notion that biomechanical properties alone cause the high bone mass phenotype observed in these mice.

We next used an osteoclast-driven model of disuse osteopenia (29, 30) to test the physiological relevance of our findings further. In this model, botulinum toxin is injected into the hind-limb muscles (quadriceps and/or calf muscle groups), which leads to transient muscle paralysis and subsequent bone loss in the ipsilateral but not contralateral tibia. Both genotypes showed similar

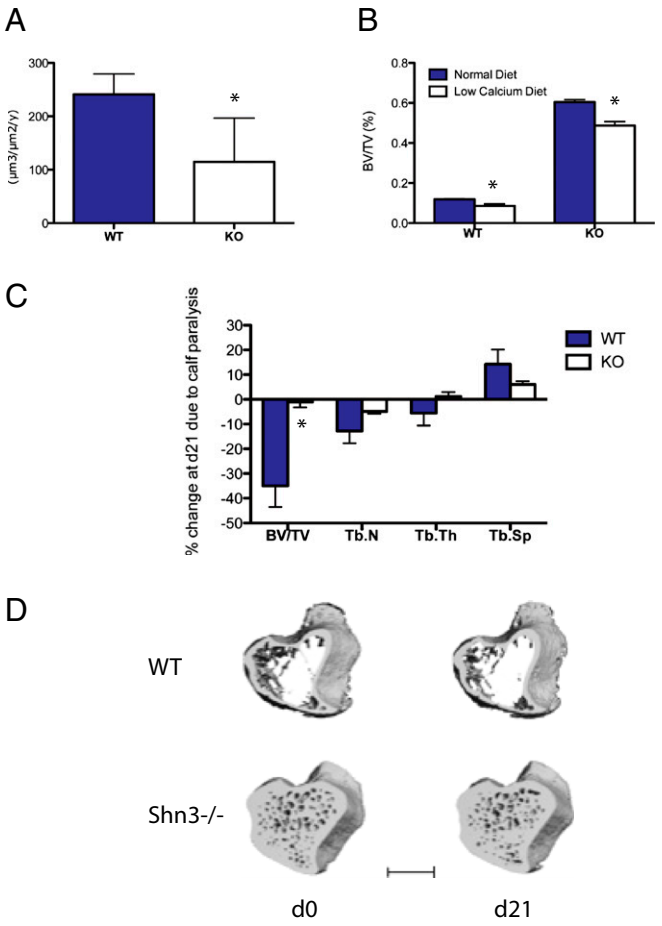

Fig. 4. In vivo analysis of Shn3-deficient mice challenged with resorptive stimuli. (*A*) Dynamic histomorphometry was performed to quantify bone formation rate in 12-wk-old WT and Shn3$^{-/-}$ (KO) animals (n = 5 mice per group). *$P < 0.05$. (*B*) Eleven-week-old WT and Shn3$^{-/-}$ (KO) mice were fed a normal or low-calcium diet for 2 wk. BV/TV in the distal femoral metaphysis was determined by micro computed tomography (μCT) (n = 5 mice per group). (*C*) Six-month-old WT (n = 6) or Shn3$^{-/-}$ (KO, n = 8) mice were injected with botulinum toxin in the calf muscle. At day 0 (just before toxin injection) and day 21, the indicated parameters were determined by μCT at metaphyseal region of the proximal tibia. Data are expressed as percent change of the indicated parameter attributable to calf paralysis. Tb.N, trabecular number; Tb.Sp, trabecular spacing; Tb.Th, trabecular thickness. (*D*) Representative μCT images depicting WT and Shn3$^{-/-}$ samples at the level of the proximal tibia during the 21-d study. WT refers to the Shn3 fl/fl genotype, whereas cKO (conditional KO) refers to Shn3 fl/fl × Prx1-Cre animals. (Scale bar: 1 mm.)

muscle atrophy (Fig. S5*D*). The subset of imaged Shn3$^{-/-}$ animals demonstrated no changes in the contralateral limb attributable to muscle paralysis (−4.2 ± 3.9%) during the 21-d study period. Although WT animals showed expected ipsilateral bone loss following this manipulation, Shn3$^{-/-}$ animals were completely protected at multiple time points (Fig. 4 *C* and *D*). This observation further supports a model in which Shn3 plays an important role in regulating bone resorption in response to a variety of physiological stimuli.

Deletion of Osteoclasts Does Not Alter the Diaphyseal High Bone Mass Phenotype in Shn3-Deficient Mice. Because we had observed reduced diaphyseal osteoclast populations in Shn3$^{-/-}$ mice (Fig. 1*D*), we wondered whether elimination of osteoclasts in the setting of Shn3 deficiency would alter this phenotype in any way. To this end, we intercrossed mice lacking Shn3 with animals harboring a conditional *NFATc1* allele and bearing an Mx1-Cre

(IFN-inducible) transgene (31). In these Shn3/NFATc1 double-KO mice bearing Mx1-Cre transgenes (and control mice lacking both genes individually), NFATc1 deletion at the age of 2 wk was achieved via polyinosinic:polycytidylic acid (poly I:C) injection (31) (*Materials and Methods*). As shown in Fig. S6 *A* and *B*, inducible deletion of NFATc1 (and therefore osteoclasts) led to a significant increase in midshaft BV/TV in WT but not Shn3-deficient mice. These data further indicate that a basal reduction in osteoclastogenesis contributes to the high bone mass phenotype seen in the absence of Shn3.

Reduced Bone Resorption in Mice Lacking Shn3 Only in Mesenchymal Cells. To interrogate further the mechanism whereby Shn3 controls the balance between bone formation and resorption in vivo, we generated mice harboring a *Shn3* allele in which exon 4 is flanked by *loxP* sites (Fig. S7*A*), hereafter called Shn3$^{f/f}$ mice. To determine definitively whether Shn3 expression in mesenchymal cells plays a role in controlling bone resorption, we intercrossed Shn3$^{f/f}$ mice with mice expressing Prx1-Cre, which expresses in the developing mesenchyme of the limbs and skull but not in the axial skeleton (32). Bone RNA harvested showed reduced Shn3 mRNA levels as expected (Fig. S7*B*). Quantitative micro quantitative computed tomography (μQCT) analysis of long bones (femur) from Shn3$^{f/f}$ mice and Shn3$^{f/f}$ mice carrying the Prx1-Cre transgene showed that transgene-carrying animals demonstrated a high bone mass phenotype nearly identical to that of mice lacking Shn3 in all cells (5) (Fig. 5 *A*–*E*). Vertebrae from Prx1-Cre Shn3$^{f/f}$ mice were identical to those of transgene-negative Shn3$^{f/f}$ mice (data not shown), confirming that Shn3 deletion causes high bone mass through a local (i.e., not humoral) mechanism. Furthermore, femurs from Prx1-Cre Shn3$^{f/f}$ mice showed improved performance in biomechanical testing compared with transgene-negative controls (Fig. S7 *C*–*E*).

Histomorphometric analysis was then performed to investigate further the effects of selective Shn3 deletion in mesenchymal cells. As was the case in global Shn3 deletion, removing Shn3 only in Prx1-expressing cells led to a robust increase in bone formation rate (Fig. 5*F*) and serum procollagen type 1 amino-terminal propeptide (P1NP) levels (Fig. 5*G*). In contrast to our previous histomorphometry data from global Shn3-deficient animals, we observed a significant increase in osteoblast numbers when Shn3 was deleted with Prx1-Cre (Fig. 5*H*).

Based on our proposed model that Shn3 deficiency in the mesenchymal lineage leads to a cell-extrinsic reduction in bone catabolism, in part, via reduced RANKL expression, we expected that Prx1-Cre Shn3$^{f/f}$ mice would show reduced osteoclast numbers and activity in addition to increased bone anabolism. Indeed, Prx1-Cre transgene-positive mice showed reduced osteoclast populations via histomorphometry (Fig. 5*I*) and reduced serum CTX levels (Fig. 5*J*). Taken together, these findings further solidify our model that Shn3 expression in mesenchymal cells directly controls osteoblastic bone formation and indirectly regulates osteoclastic bone resorption.

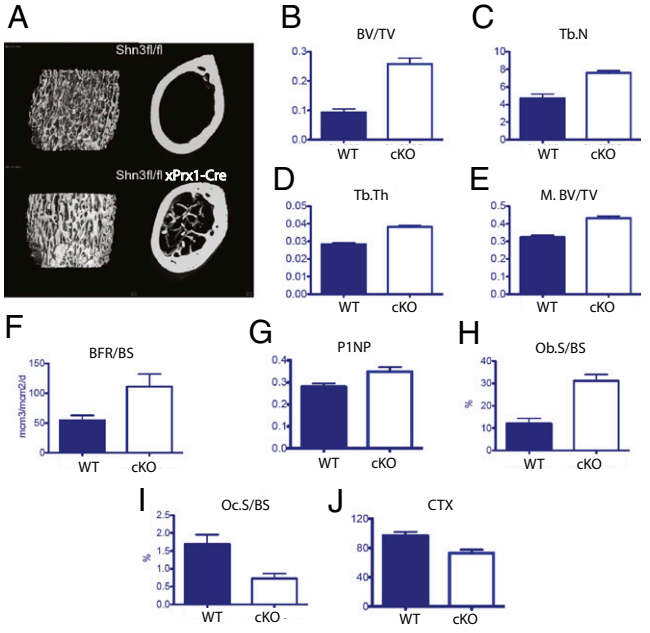

Fig. 5. Deletion of Shn3 in Prx1-expressing cells leads to a high bone mass phenotype with decreased bone catabolism in vivo. (*A*) Representative metaphyseal (*Left*) and midshaft (*Right*) microcomputed tomography (micro-CT) images of mice of the indicated genotype. (*B*–*D*) Micro-CT–derived metaphyseal BV/TV, trabecular number (Tb.N), and trabecular thickness (Tb.Th) of mice of the indicated genotype. (*E*) Micro-CT–derived diaphyseal (midshaft) BV/TV (M.BV/TV) of mice of the indicated genotype. Osteoblastic parameters in vivo are provided as determined by dynamic (*F*) and static histomorphometry (*H*), as well as serum P1NP levels (*G*). BFR/BS, bone formation rate/bone surface; Ob.S/BS, osteoblast surface/bone surface. Osteoclastic parameters in vivo are determined by static histomorphometry (*I*) and serum CTX levels (*J*). Oc.S/BS, octeoclast surface/bone surface. Comparison of Prx1-Cre transgene-negative and -positive animals for all parameters shown. $P < 0.05$.

Discussion

We had previously observed that Shn3 functions as an important inhibitor of osteoblastic bone formation (5). Here, we show that the dramatic high bone mass phenotype seen in Shn3-deficient animals is likely attributable to both increased bone formation and reduced bone resorption. Shn3-deficiency seems to uncouple these processes.

Recently, it has been suggested that Shn3 (also known as ZAS3) may play a cell-intrinsic role in regulating osteoclastogenesis by regulating receptor activator of nuclear factor-κB signaling (33). Consistent with our findings, these authors observed increased bone mass with increased fracture resistance in an independent model of germline Shn3 deletion. Similar to our findings, Liu et al. (33) observed decreased numbers of osteoclasts in vivo. However, we believe that our current findings of persistent high bone mass phenotype in WT animals receiving Shn3-deficient BM transplantation (Fig. S1*B*) and, more importantly, a high bone mass phenotype in mice lacking Shn3 selectively in mesenchymal cells (Fig. 5) highlight that the predominant effect of Shn3 deficiency in vivo maps to the mesenchymal, rather than hematopoietic, compartment. Moreover, in our previous experiments (5), we found no defect whatsoever in osteoclast differentiation and function comparing WT and Shn3-deficient BM cells.

It is interesting that Shn3 deficiency leads to qualitative reductions in osteoclasts in calvariae and diaphyseal bone but not in metaphyseal regions. This observation suggests that different cell populations are responsible for RANKL expression and osteoclastogenesis at these different anatomical sites. Indeed, it has previously been suggested that hypertrophic chondrocytes play a critical role in driving the differentiation of metaphyseal osteoclasts/chondroclasts during development, a finding that is consistent with preserved expression of RANKL in these cells in situ in Shn3$^{-/-}$ mice (34, 35). More recently, cell type-specific RANKL deletion has shown that hypertrophic chondrocytes play a major role in regulating metaphyseal osteoclasts (19), whereas late-stage [dentin matrix protein 1 (DMP1)-expressing] osteoblasts/osteocytes are more important sources of RANKL for osteoclasts involved in adult skeletal remodeling (18, 19). Future studies are required to interrogate the activity of Shn3 in DMP1-expressing bone cells.

We found that Shn3 controls RANKL expression, at least in part, through a regulatory region 76 kb upstream of the transcription start site. Just as Shn3 interacts with c-Jun to coactivate AP-1 complexes in the context of the IL-2 gene in T cells (6), Shn3 seems to function as a context-dependent transcriptional coactivator in the setting of the RANKL gene in mesenchymal cells. Little is known about its structure/function relationship, and the mechanism whereby it functions as a transcriptional

coactivator in certain situations. It is interesting that Shn3, like ATF4, is required for RANKL up-regulation in osteoblastic cells in response to isoproterenol but not PTH (36). Future work is required to determine if there is a relationship between Shn3 and ATF4.

Mice lacking Shn3 are completely protected from bone loss induced by muscle paralysis achieved via Botox-induced transient paralysis of calf muscles. Bone loss in this model is osteoclast-driven, as evidenced by complete protection observed in the absence of NFATc1 (30). Although it is clear that osteoclastic bone resorption via RANKL is critical for bone loss in the model, the cellular source of RANKL remains unclear. Recent work suggests that an intercellular communication pathway between osteocytes, RANKL-expressing cells, and osteoclasts involving the secreted protein sclerostin may be involved (37, 38). Mice lacking RANKL in DMP1-expressing cells are protected from bone loss in a similar model (19). Future studies will be required to determine what, if any, role there is for Shn3 in mechanotransduction in osteocytes.

In summary, we have shown that the high bone mass phenotype of Shn3-deficient mice is likely attributable to a combination of increased bone formation and reduced bone resorption. We do note that it is difficult to conclude from our current study which aspect of the Shn3-deficient phenotype (increased bone formation or reduced bone resorption) is more important for the overall high bone mass phenotype. Additional studies are required to address this important outstanding question definitely. That being said, it is provocative that the aged Shn3-deficient mice maintain a dramatic high bone mass phenotype yet show reduced bone formation rates. Based on our findings, one would predict that small-molecule Shn3 inhibitors would increase bone mass through both of these mechanisms.

Materials and Methods

Mice. Shn3-deficient animals were as previously described (5). Conditional Shn3 KO mice were generated at Taconic and on a C57/BL6 background. Prx-1-Cre mice were purchased from the Jackson Laboratory. Conditional NFATc1-deficient mice were as described (31) and intercrossed with $Shn3^{-/-}$ mice.

Serum Measurements. Levels of Pyd (Quidel), CTX (IDS), RANKL (R&D Systems), and calcium (BioAssay) were determined per the instructions of the manufacturers.

Histology and Immunohistochemistry. Decalcified femur sections were stained with RANKL antibodies (sc-7628; Santa Cruz Biotechnology) and TRAP (Sigma).

Osteoblast/Osteoclast Cocultures. Calvarial osteoblasts were grown in medium supplemented only with 10% (vol/vol) FCS and antibiotics. Osteoclast precursors were isolated from adult male BM cells precultured in macrophage-colony stimulating factor (M-CSF) and isolated by Histopaque 1083 (Sigma) gradient centrifugation.

Luciferase Assays and Coimmunoprecipitations. Experiments were performed using previously described methods (5).

In Vivo Muscle Paralysis. Experiments were performed as previously described (29) using 6-mo-old WT and $Shn3^{-/-}$ mice on a BALB/c genetic background. Additional details are provided in *SI Materials and Methods*.

ACKNOWLEDGMENTS. We thank Dorothy Zhang for histological preparations, Nicholas Brady and Mary Bouxsein for μCT analyses, David Burr for histomorphometric analysis, Merck pharmaceuticals for assistance in generating the $Shn3^{f/f}$ mice, and Charles O'Brien for the RANKL reporter reagents. This work was supported by National Institutes of Health Grants HD055601 (to L.H.G.) and K99AR055668 (to D.C.J.). A.O.A. holds a Career Award for Medical Scientists from the Burroughs Wellcome Fund and was supported by Grants K08AR054859 and R01AR060363 from the National Institute of Arthritis and Musculoskeletal and Skin Diseases.

1. Wu LC (2002) ZAS: C2H2 zinc finger proteins involved in growth and development. *Gene Expr* 10:137–152.
2. Wu LC, et al. (1996) The mouse DNA binding protein Rc for the kappa B motif of transcription and for the V(D)J recombination signal sequences contains composite DNA-protein interaction domains and belongs to a new family of large transcriptional proteins. *Genomics* 35:415–424.
3. Allen CE, Mak CH, Wu LC (2002) The kappa B transcriptional enhancer motif and signal sequences of V(D)J recombination are targets for the zinc finger protein HIVEP3/KRC: A site selection amplification binding study. *BMC Immunol* 3:10.
4. Oukka M, et al. (2002) A mammalian homolog of Drosophila schnurri, KRC, regulates TNF receptor-driven responses and interacts with TRAF2. *Mol Cell* 9: 121–131.
5. Jones DC, et al. (2006) Regulation of adult bone mass by the zinc finger adapter protein Schnurri-3. *Science* 312:1223–1227.
6. Oukka M, Wein MN, Glimcher LH (2004) Schnurri-3 (KRC) interacts with c-Jun to regulate the IL-2 gene in T cells. *J Exp Med* 199:15–24.
7. Erlebacher A, Filvaroff EH, Gitelman SE, Derynck R (1995) Toward a molecular understanding of skeletal development. *Cell* 80:371–378.
8. Matsuo K, Irie N (2008) Osteoclast-osteoblast communication. *Arch Biochem Biophys* 473:201–209.
9. Martin T, Gooi JH, Sims NA (2009) Molecular mechanisms in coupling of bone formation to resorption. *Crit Rev Eukaryot Gene Expr* 19:73–88.
10. Saag KG, et al. (2007) Teriparatide or alendronate in glucocorticoid-induced osteoporosis. *N Engl J Med* 357:2028–2039.
11. Brown JP, et al. (2009) Comparison of the effect of denosumab and alendronate on BMD and biochemical markers of bone turnover in postmenopausal women with low bone mass: A randomized, blinded, phase 3 trial. *J Bone Miner Res* 24:153–161.
12. Elefteriou F, et al. (2006) ATF4 mediation of NF1 functions in osteoblast reveals a nutritional basis for congenital skeletal dysplasiae. *Cell Metab* 4:441–451.
13. Bennett CN, et al. (2007) Wnt10b increases postnatal bone formation by enhancing osteoblast differentiation. *J Bone Miner Res* 22:1924–1932.
14. Li X, et al. (2008) Targeted deletion of the sclerostin gene in mice results in increased bone formation and bone strength. *J Bone Miner Res* 23:860–869.
15. Akune T, et al. (2004) PPARgamma insufficiency enhances osteogenesis through osteoblast formation from bone marrow progenitors. *J Clin Invest* 113:846–855.
16. Sabatakos G, et al. (2000) Overexpression of DeltaFosB transcription factor(s) increases bone formation and inhibits adipogenesis. *Nat Med* 6:985–990.
17. Wada T, Nakashima T, Hiroshi N, Penninger JM (2006) RANKL-RANK signaling in osteoclastogenesis and bone disease. *Trends Mol Med* 12:17–25.
18. Nakashima T, et al. (2011) Evidence for osteocyte regulation of bone homeostasis through RANKL expression. *Nat Med* 17:1231–1234.
19. Xiong J, et al. (2011) Matrix-embedded cells control osteoclast formation. *Nat Med* 17:1235–1241.
20. Takahashi N, et al. (1988) Osteoblastic cells are involved in osteoclast formation. *Endocrinology* 123:2600–2602.
21. O'Brien CA (2010) Control of RANKL gene expression. *Bone* 46:911–919.
22. Sato K, et al. (2006) Th17 functions as an osteoclastogenic helper T cell subset that links T cell activation and bone destruction. *J Exp Med* 203:2673–2682.
23. Thomas GP, Baker SU, Eisman JA, Gardiner EM (2001) Changing RANKL/OPG mRNA expression in differentiating murine primary osteoblasts. *J Endocrinol* 170: 451–460.
24. Kim S, Yamazaki M, Zella LA, Shevde NK, Pike JW (2006) Activation of receptor activator of NF-kappaB ligand gene expression by 1,25-dihydroxyvitamin D3 is mediated through multiple long-range enhancers. *Mol Cell Biol* 26:6469–6486.
25. Fu Q, Manolagas SC, O'Brien CA (2006) Parathyroid hormone controls receptor activator of NF-kappaB ligand gene expression via a distant transcriptional enhancer. *Mol Cell Biol* 26:6453–6468.
26. Galli C, et al. (2008) Targeted deletion of a distant transcriptional enhancer of the receptor activator of nuclear factor-kappaB ligand gene reduces bone remodeling and increases bone mass. *Endocrinology* 149:146–153.
27. Kim S, et al. (2007) Multiple enhancer regions located at significant distances upstream of the transcriptional start site mediate RANKL gene expression in response to 1,25-dihydroxyvitamin D3. *J Steroid Biochem Mol Biol* 103:430–434.
28. Aoki K, et al. (2006) A TNF receptor loop peptide mimic blocks RANK ligand-induced signaling, bone resorption, and bone loss. *J Clin Invest* 116:1525–1534.
29. Warner SE, et al. (2006) Botox induced muscle paralysis rapidly degrades bone. *Bone* 38:257–264.
30. Aliprantis AO, et al., Transient muscle paralysis degrades bone via rapid osteoclastogenesis. *FASEB J* 26:1110–1118.
31. Aliprantis AO, et al. (2008) NFATc1 in mice represses osteoprotegerin during osteoclastogenesis and dissociates systemic osteopenia from inflammation in cherubism. *J Clin Invest* 118:3775–3789.
32. Logan M, et al. (2002) Expression of Cre Recombinase in the developing mouse limb bud driven by a Prxl enhancer. *Genesis* 33:77–80.
33. Liu S, et al. (2011) The large zinc finger protein ZAS3 is a critical modulator of osteoclastogenesis. *PLoS ONE* 6:e17161.
34. Masuyama R, et al. (2006) Vitamin D receptor in chondrocytes promotes osteoclastogenesis and regulates FGF23 production in osteoblasts. *J Clin Invest* 116:3150–3159.
35. Usui M, et al. (2008) Murine and chicken chondrocytes regulate osteoclastogenesis by producing RANKL in response to BMP2. *J Bone Miner Res* 23:314–325.
36. Elefteriou F, et al. (2005) Leptin regulation of bone resorption by the sympathetic nervous system and CART. *Nature* 434:514–520.
37. Lin C, et al. (2009) Sclerostin mediates bone response to mechanical unloading through antagonizing Wnt/beta-catenin signaling. *J Bone Miner Res* 24:1651–1661.
38. Tatsumi S, et al. (2007) Targeted ablation of osteocytes induces osteoporosis with defective mechanotransduction. *Cell Metab* 5:464–475.

Supporting Information

Wein et al. 10.1073/pnas.1205848109

SI Materials and Methods

Mice. The generation and characterization of $Shn3^{-/-}$ animals were previously described (1). For this study, mice were backcrossed to a BALB/c background for >10 generations, and age- and sex-matched BALB/c WT mice were used as controls. Conditional Shn3 KO mice were generated at Taconic and maintained on a C57/BL6 background. Prx1-Cre mice on a C57/BL6 background were purchased from the Jackson Laboratory. Conditional NFATc1-deficient mice were as previously described (2). Briefly, $NFATc1^{fl/fl}$ $Shn3^{+/-}$ $MxCre^{+}$ mice were crossed with $NFATc1^{fl/fl}$ $Shn3^{+/-}$ $MxCre^{-}$ mice. Before genotyping at postnatal days 10, 12, and 14, all mice were treated with polyinosinic:polycytidylic acid (poly dI:C) (2). Animals were killed at 10 wk of age, and midshaft femur total BV/TV was analyzed by microcomputed tomography (micro-CT).

Serum Measurements. Serum was collected from WT and $Shn3^{-/-}$ mice and stored at −80 °C. Samples for comparison were always collected at the same time of day. Measurements for Pyd (Quidel), CTX (IDS), calcium (BioAssay), and RANKL (R&D Systems) were performed per the instructions of the manufacturers.

Whole-Mount TRAP Histochemistry. Calvariae from 8-wk-old mice were dissected, soft tissue was removed, and the calvariae were fixed in 100% methanol for 5 min. Bones were thoroughly washed in water, and TRAP staining was performed per the instructions of the manufacturer (Sigma).

Histology and Immunohistochemistry. Femurs were isolated from 8-wk-old mice, decalcified, paraffin-embedded, and sectioned. Sections were dewaxed and blocked in 3% H_2O_2 in PBS for 20 min, and TRAP staining was performed per the manufacturer's protocol. For subsequent RANKL immunohistochemistry, proteinase K treatment was then performed. Sections were blocked in 3% donkey serum with 1% BSA and 0.1% Triton X-100 for 1 h at room temperature and then incubated with RANKL antibody (sc-7628; Santa Cruz Biotechnology) at 4 °C overnight. Detection was performed with donkey anti-goat horseradish peroxidase (HRP), trichostatin A (TSA)-biotin, streptavidin-HRP, and diaminobenzidine (DAB) amplification. Sections were counterstained in hematoxylin and mounted.

Osteoblast/Osteoclast Cocultures. Calvarial osteoblasts were derived from P2–P5 neonatal BALB/c mice as previously described (1) and cultured in α-MEM supplemented only with 10% FCS and antibiotics (penicillin/streptomycin). Cells were allowed to reach confluency, and were then split into 96-well plates at a density of 30,000 cells/mL. Two days later, osteoclast precursors were added in the presence of calciotropic agents. Vitamin D (Sigma) was added at a concentration of 10 nM. PGE2 (Calbiochem) was used at a concentration of 10 μM. PTH (Sigma) was used at 10 nM. Isoproterenol (Sigma) was used at 10 μM. Anti-OPG antibody (R&D Systems) was used at 10 μg/mL. Osteoclast precursors were derived from adult male BALB/c mice. Briefly, long bones were carefully dissected, marrow was flushed, and all cells were plated overnight in α-MEM plus 10% FCS with macrophage-colony stimulating factor (M-CSF) (10 ng/mL; Peprotech). Eighteen hours later, nonadherent cells were collected and mononuclear osteoclast precursor cells were purified using Histopaque 1083 gradient (Sigma) centrifugation. Four to five days later, tissue culture supernatant was harvested from TRAP assay (Sigma) or cells were fixed and stained for microscopy. Secreted TRAP was used to quantify osteoclastogenesis in these experiments because we found this led to a more robust and reproducible quantification than manual counting of osteoclasts.

RNA Isolation and Real-Time Quantitative PCR Assay. RNA was isolated from adult calvariae and tissue culture using TRIzol (Invitrogen) reagent per the instructions of the manufacturer. To analyze gene expression, cDNA was synthesized and quantitative PCR assays for actin, RANKL, Runx2, OPG, osteocalcin (OCN), Col1a1, calcitonin receptor, and cathepsin K were performed as described (1). Primer sequences are available on request.

SV40-Transformed Osteoblast Cell Lines. WT and $Shn3^{-/-}$ primary calvarial osteoblasts were transformed with a plasmid encoding the SV40 large T antigen, and various transformed subclones were obtained and characterized. Cells expressing osteoblastic markers (Runx2 and Osterix) were used for further studies. WT cells were infected with control, Shn3 shRNA, and Shn3 overexpression lentiviruses containing a puromycin resistance gene. Infected cells were selected with puromycin, and RNA was harvested and analyzed as above. We used a combination of primary calvarial osteoblasts and SV40-transformed osteoblastic cells in these experiments because of different expression levels of receptors for these agents in various cell types.

Luciferase Reporter Assays. C3HT101/2 cells were transiently transfected as previously described (1). Luciferase reporters were used containing the proximal OPG promoter (3) and the distal RANKL upstream enhancer region with mutated CREB binding sites (4). Forty-eight hours after transfection (Effectene; Qiagen), cells were harvested and firefly and renilla luciferase activities were determined on a luminometer using Promega dual-luciferase reagent.

Coimmunoprecipitation. 293T cells were transfected with Shn3 (1), HA-Runx2 (a gift from Jane Lian, University of Massachusetts, Worcester, MA), and HA-CREB (a gift from Michael Greenberg, Children's Hospital, Boston, MA). Forty-eight hours later, cells were lysed in buffer [200 mM NaCl, 20 mM Tris·HCl (pH 8.0), 0.5% Triton X-100] supplemented with protease inhibitors. Lysates were incubated with anti–HA-coupled agarose (F7; Santa Cruz Biotechnology) overnight at 4 °C. Immune complexes were washed three times in lysis buffer, and precipitated proteins were resolved by SDS/PAGE followed by immunoblotting for Shn3 or HA.

BM Transplantation. WT or $Shn3^{-/-}$ mice on a pure (backcrossed for >10 generations) BALB/c genetic background were lethally irradiated and rescued with 0.5×10^6 BM cells via tail vein injection from either WT or $Shn3^{-/-}$ mice. Ten weeks later, chimeras were killed, splenic B cells were harvested using $CD19^{+}$ selection (Miltenyi), and genomic DNA was analyzed by PCR assay using previously published primer sequences (1). At the same time, femurs were harvested and analyzed by micro computed tomography (μCT).

Th17 Cell Generation and RANKL (CD254) FACS. Spleen and lymph node were harvested from adult WT or $Shn3^{-/-}$ C57B/6 animals. RBCs were lysed, and single-cell suspensions were prepared according to standard methods. $CD4^{-}$ selection was performed using Robosep (Stem Cell) according to the manufacturer's instructions. Naive $CD4^{+}CD62L^{high}CD25^{-}$ cells were purified by cell sorting and incubated at a 1:3 ratio with irradiated spleno-

cytes (2,000 rad) in RPMI in the presence of anti-CD3, TGF-β1 (2 ng/mL; R&D Systems), IL-6 (20 ng/mL; R&D Systems), and anti–IL-4 (10 μg/mL) and anti–IFN-γ (10 μg/mL) antibodies. Two to three days later, cells were collected and transferred into fresh medium containing the aforementioned cytokines and antibodies, except in the absence of anti-CD3, cells were then split at a 1:2 ratio as needed. Two to three days later, cells were collected and restimulated with phorbol 12-myristate 13-acetate (PMA)/ionomycin for 30 min and fluorescence-activated cell sorter staining with isotype control or anti-RANKL (CD254; 510003; Biolegend) antibody.

Low-Calcium Diet. WT or Shn3$^{-/-}$ mice on a BALB/c genetic background were placed on either a control (0.6% Ca, 0.4% P; TD.97191; Harlan Tekland) or low-calcium (0.02% Ca, 0.4% P; TD.02279; Harlan Tekland) diet from the age of 11–13 wk. Animals were then killed, and femurs were harvested and analyzed by μCT. PTH levels were not measured because serum levels of calcium and phosphorus were comparable in animals of both genotypes on both diets.

In Vivo Transient Muscle Paralysis Model. Under isoflurane anesthesia, each mouse was weighed on day 0 and given a single i.m. injection of botulinum toxin A (2 U per 100 g, 20-μL final volume of Botox; Allergan) or a saline injection of equivalent volume in the right calf muscle group. All mice received an s.c. injection of saline (800 μL) for each of the next 4 d to ensure sufficient hydration. At 24 h postinjection, all mice were visually examined for calf paralysis by assessing whether the mice could extend their toes or demonstrate ankle plantar flexion during transient tail suspension. Mice were group-housed with free ambulation and received food and water ad libitum per procedures approved by the University of Washington Institutional Animal Care and Use Committee.

Micro-CT Imaging and Analysis. In vivo imaging was conducted with a high-resolution micro-CT scanner (10.5-μm voxel resolution; Scanco vivaCT 40). While anesthetized with isoflurane, each mouse underwent imaging of the right proximal tibia metaphysis (i.e., trabecular bone assessment) and right tibia middiaphysis (i.e., cortical bone assessment) on day 0. A subset of Shn3 KO mice (n = 4) also underwent baseline imaging of the left (contralateral) tibia metaphysis and tibia diaphysis. Botox (or saline) intervention occurred following imaging on day 0 while the mice were still under anesthesia. Final imaging was repeated for each mouse on day 21.

Standard image analysis procedures were used to determine trabecular bone and cortical bone parameters (5). User-defined contour lines were drawn every 15 slices, and interim contour lines were morphed along the entire analysis region using algorithms developed by Scanco. For the proximal tibia metaphysis, we determined trabecular fraction (BV/TV), trabecular number (mm), trabecular thickness (mm), and trabecular spacing (mm) within a 0.8-mm region initiating at the distal edge of the metaphyseal growth plate for each mouse at day 0 vs. day 21. Tibia middiaphysis cortical bone morphology was assessed for a 1.0-mm region centered 1.2 mm proximal to the tibia-fibula junction. Cortical bone outcome measures included periosteal volume (mm^3), cortical volume (mm^3), endocortical volume (mm^3), and cortical thickness (mm^3).

Biomechanical Testing. Biomechanical testing of WT (Shn3 f/f) and Shn3 conditional KO (Shn3 f/f × Prx1-Cre) femurs was performed using a BioDent Bio-Indenter according to the instructions of the manufacturer to obtain parameters that included indentation distance increase (μm), mean energy dissipated (μJ), and unloading stiffness (N/μm). Femurs from 4 male mice per genotype were tested.

1. Jones DC, et al. (2006) Regulation of adult bone mass by the zinc finger adapter protein Schnurri-3. *Science* 312:1223–1227.
2. Aliprantis AO, et al. (2008) NFATc1 in mice represses osteoprotegerin during osteoclastogenesis and dissociates systemic osteopenia from inflammation in cherubism. *J Clin Invest* 118:3775–3789.
3. Kieslinger M, et al. (2005) EBF2 regulates osteoblast-dependent differentiation of osteoclasts. *Dev Cell* 9:757–767.
4. Fu Q, Manolagas SC, O'Brien CA (2006) Parathyroid hormone controls receptor activator of NF-kappaB ligand gene expression via a distant transcriptional enhancer. *Mol Cell Biol* 26:6453–6468.
5. Warner SE, et al. (2006) Botox induced muscle paralysis rapidly degrades bone. *Bone* 38:257–264.

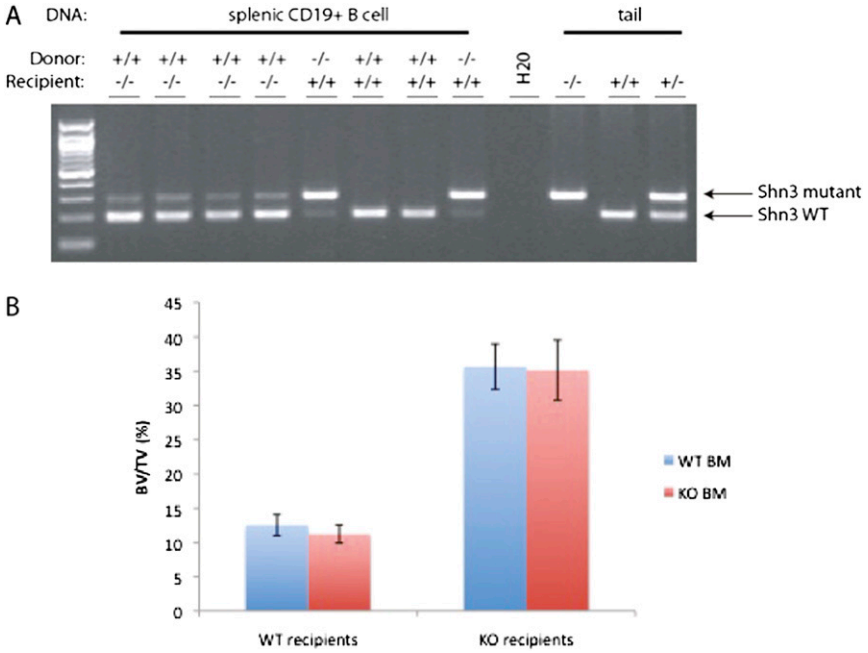

Fig. S1. Reciprocal BM transplantation. (*A*) Genomic DNA was purified from CD19^{+} B cells from the indicated radiation chimeras, and a PCR assay was performed to assess the degree of hematopoietic chimerism qualitatively. (*B*) Distal femoral BV/TV was determined from the indicated radiation chimeras. Error bars represent SD of $n = 2$ WT recipients and $n = 4$ KO recipients per experimental group.

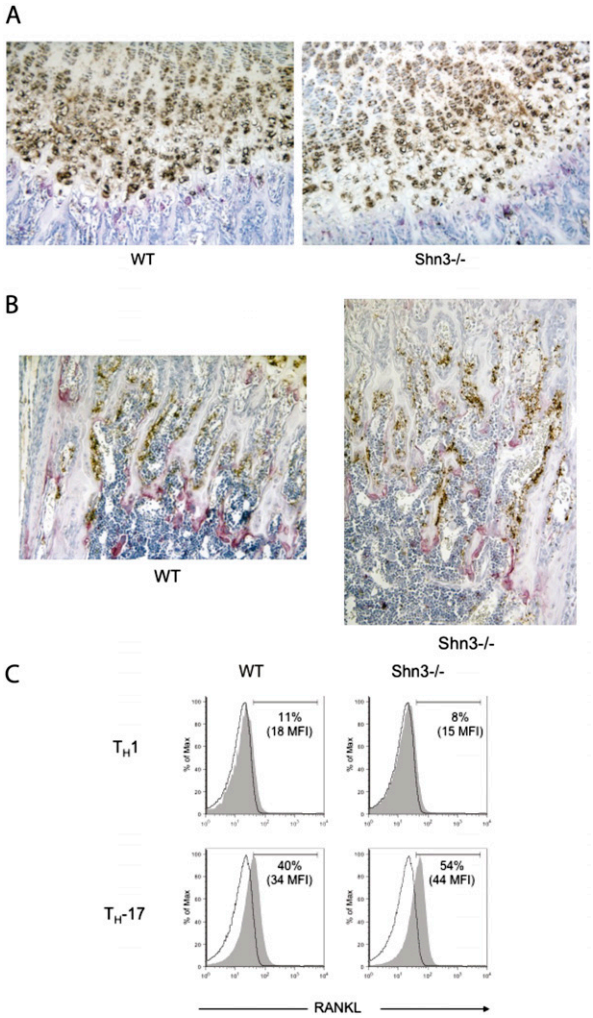

Fig. S2. RANKL expression in hypertrophic chondrocytes and Th17 cells. (*A*) p10 sections from WT or Shn3$^{-/-}$ animals were processed for RANKL immunohistochemistry (brown) and TRAP histochemistry (red) simultaneously. Comparable RANKL expression was observed in hypertrophic chondrocytes from WT and Shn3$^{-/-}$ sections. (*B*) Representative sections from similar animals shown at the level of the metaphysis. Again, comparable RANKL expression in metaphyseal bone-lining cells and TRAP activity were observed. (*C*) Th1 (T_H1) and Th17 (T_H17) cells were generated from WT and Shn3$^{-/-}$ mice, and surface RANKL expression was determined by fluorescence-activated cell sorting. No significant differences were observed comparing WT and Shn3$^{-/-}$ Th17 cells. MFI. (Magnification: 10× in *A* and *B*.)

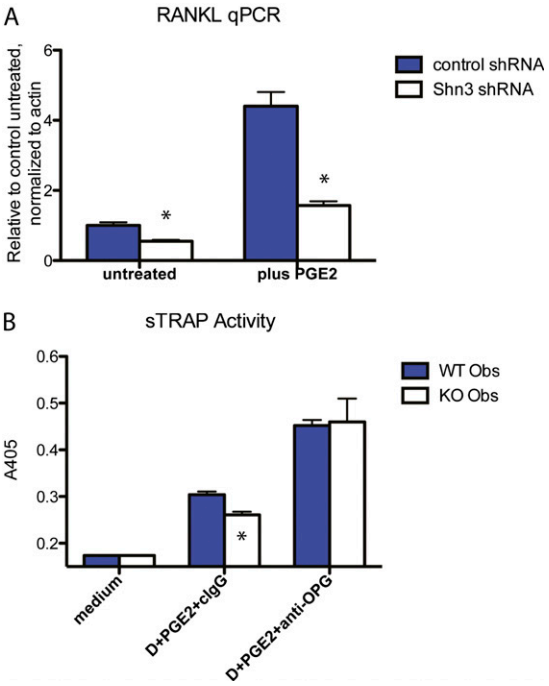

Fig. S3. (*A*) RANKL mRNA levels were determined by quantitative PCR (qPCR) assay in SV40-transformed osteoblast cell lines transduced with control shRNA-expressing lentivirus or lentivirus expressing shRNA targeting Shn3. Cells were harvested following treatment with PGE2 (10 μM) for 3 h. Data are expressed as mRNA levels relative to control untreated sample, and all samples were normalized to actin. Error bars represent SD of experimental triplicates. Data shown are representative of three independent experiments. $*P < 0.05$. (*B*) Cocultures were performed using calvarial osteoblasts from WT or Shn3$^{-/-}$ (KO) neonates, with WT BM responder cells, and in the presence of the indicated calciotropic agents and neutralizing anti-OPG antibody. Secreted TRAP activity was determined at day 5. Obs. Error bars represent experimental triplicates. Data shown are representative of three independent experiments. $*P < 0.05$.

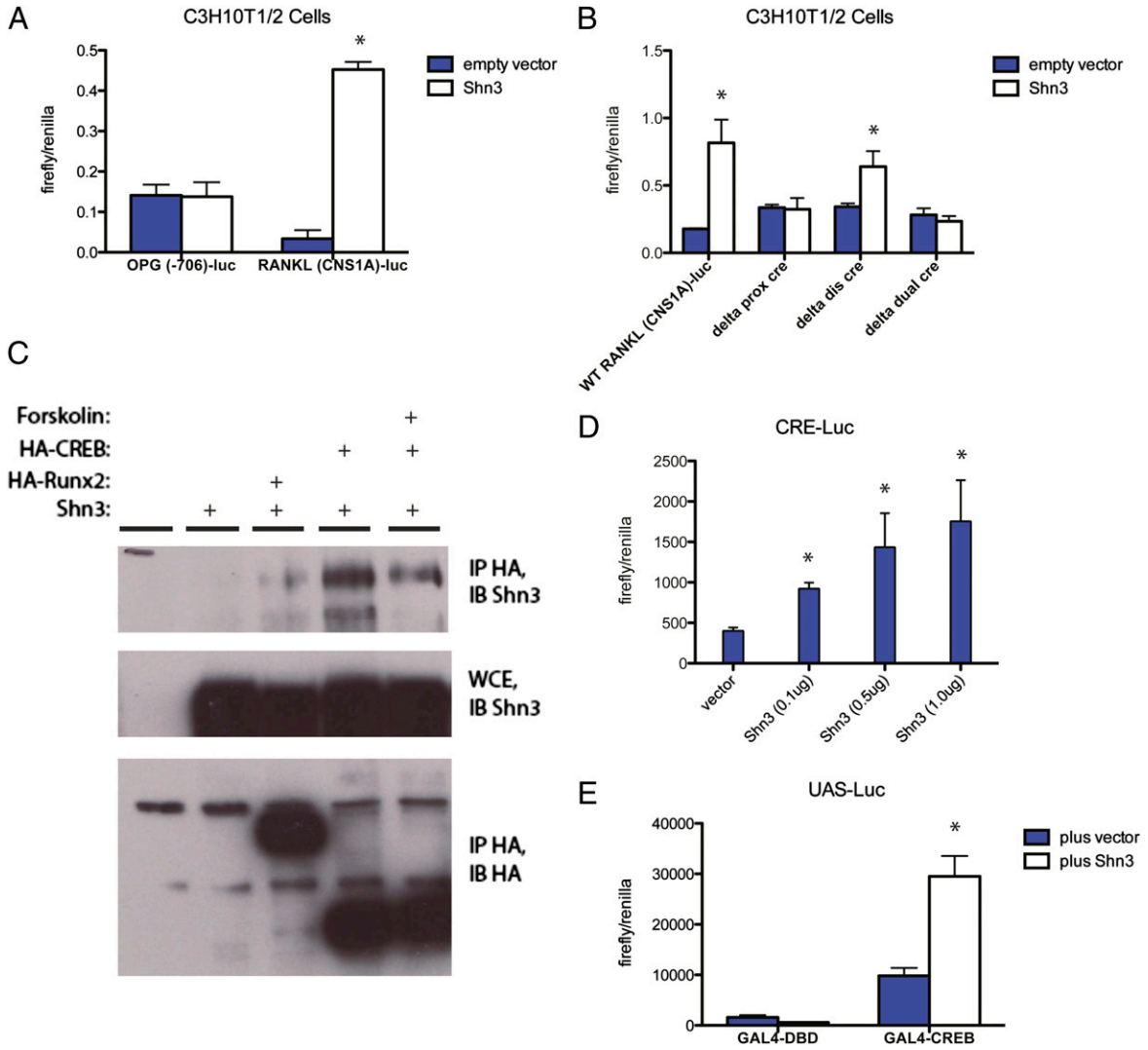

Fig. S4. Shn3 can regulate RANKL gene expression through an upstream regulatory region and CREB. (*A*) C3H10T1/2 cells were transiently transfected with a luciferase reporter element containing either the proximal OPG promoter or the RANKL upstream regulatory element CNS1A with either empty vector or Shn3. Firefly and renilla luciferase activities were determined after 48 h. Error bars represent the firefly/renilla ratio from triplicate experimental wells. (*B*) C3H10T1/2 cells were transfected as in *A* with the indicated CNS1A-luciferase reporter constructs. (*C*) 293T cells were transfected with the indicated combinations of Shn3 and HA-tagged versions of either CREB or Runx2. IB, immunoblot; IP, immunoprecipitation; WCE, whole cell extract. C3H10T1/2 cells were transfected with the indicated combinations of CRE-Luc reporter, empty vector, and Shn3 (*D*) and UAS-Luc reporter, Gal4-DBD, Gal4-CREB, empty vector, and Shn3 (*E*). Firefly and renilla luciferase activities were determined after 48 h. Error bars represent the firefly/renilla ratio from triplicate experimental wells. $*P < 0.05$ compared with empty vector. Each experiment was performed three independent times with similar results.

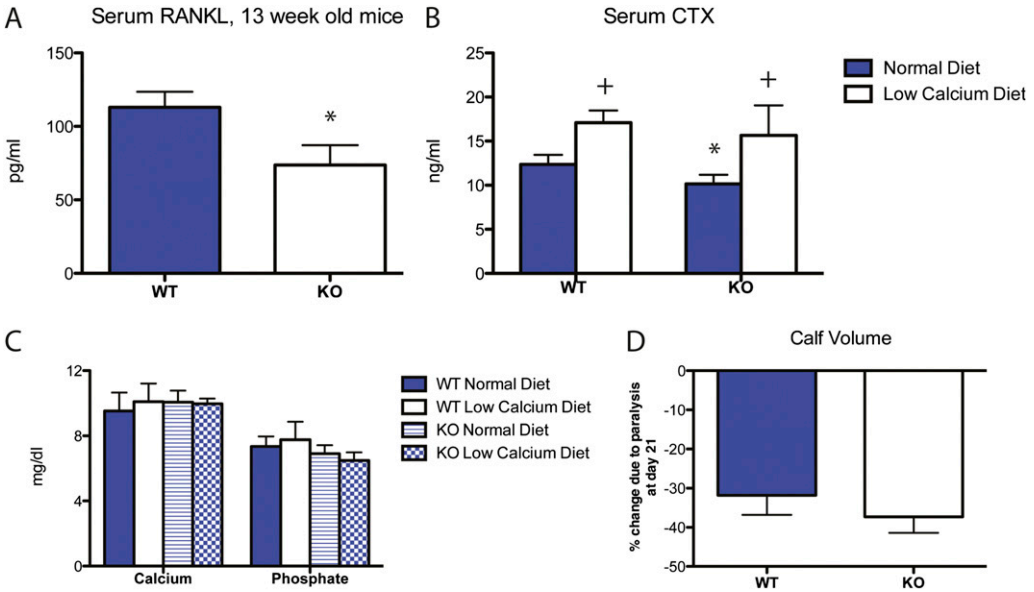

Fig. S5. (*A*) Serum RANKL levels were determined from 13-wk-old WT and Shn3-deficient (KO) mice ($n = 5$ mice per group). *$P < 0.03$. (*B*) Serum CTX levels were determined from WT and Shn3$^{-/-}$ (KO) animals after 2 wk of the indicated diet ($n = 4$ mice per experimental group). *$P < 0.02$ comparing WT normal diet with KO normal diet. $^{+}P < 0.05$ comparing normal diet with low-calcium diet within each genotype. (*C*) Serum calcium and phosphate levels were determined from WT and KO animals fed the indicated diet for 2 wk. No significant differences were observed ($n = 4$ mice per experimental group). (*D*) Volumetric analysis of calf volume atrophy in WT ($n = 6$) or Shn3$^{-/-}$ (KO, $n = 8$) mice following local Botox injection.

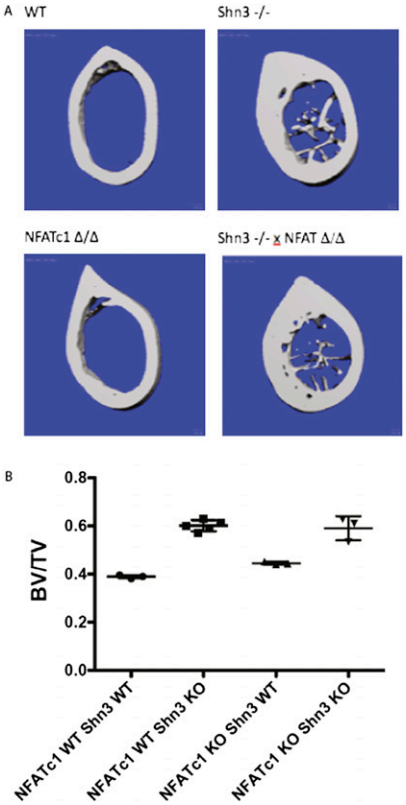

Fig. S6. Effect of inducible deletion of osteoclasts on the diaphyseal phenotype of Shn3-deficient mice. (*A*) Representative midshaft micro-CT images from mice of the indicated genotype. (*B*) Midshaft BV/TV of 10-wk-old Shn3 mice of the indicated genotype with or without osteoclasts (based on NFATc1 genotype). *P* values for two-tailed unpaired Student *t* tests: NFATc1 WT Shn3 WT vs. NFATc1 WT Shn3 KO, $P < 0.0001$; NFATc1 WT Shn3 WT vs. NFATc1 KO Shn3 WT, $P = 0.0005$; NFATc1 WT Shn3 KO vs. NFATc1 KO Shn3 KO, $P = 0.6981$ ($n = 4$ mice per genotype).

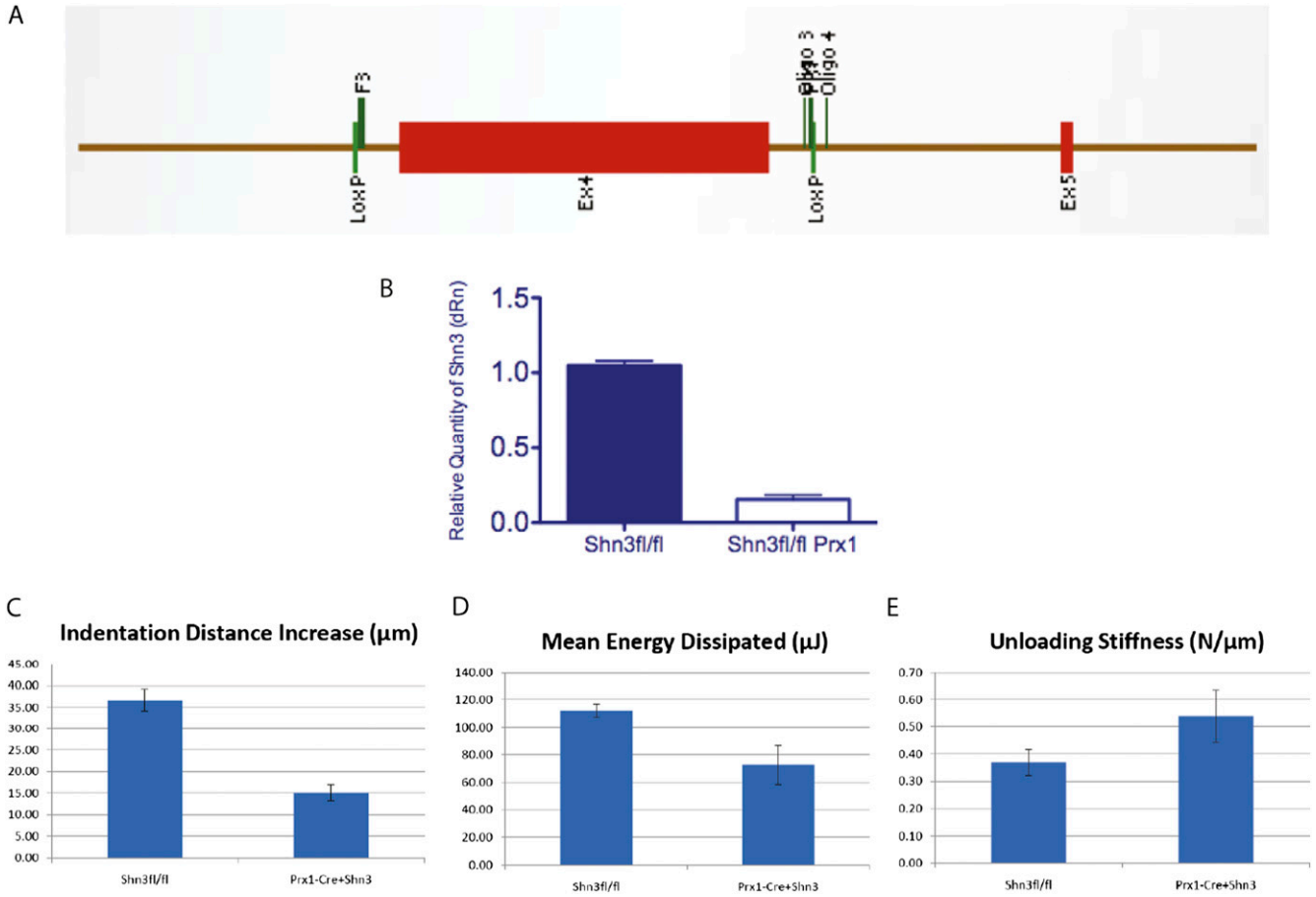

Fig. S7. (*A*) Schema for targeted allele. LoxP sites flank exon 4, which contains the majority of the coding region for the Shn3 protein. (*B*) Quantitative PCR data showing reduced Shn3 expression in Prx1-Cre transgene-positive mice. (*C–E*) Biomechanical parameters tested from Shn3 f/f transgene-negative (*Left*) and transgene-positive (*Right*) mice (n = 4 were tested per group). For all parameters shown, $P < 0.05$ comparing transgene-negative and transgene-positive groups.